Design and performance analysis of ORC centrifugal pumps

PIOTR KLIMASZEWSKI*
PIOTR KLONOWICZ
PIOTR LAMPART
ŁUKASZ WITANOWSKI
DAWID ZANIEWSKI
ŁUKASZ JĘDRZEJEWSKI
TOMASZ SUCHOCKI

Institute of Fluid-Flow Machinery, Polish Academy of Sciences, Fiszera 14, 80-231 Gdańsk, Poland

Abstract The purpose of this work is to design and determine the per-formance of a prototype centrifugal pump impeller for an organic Rank-ine cycle (ORC) power plant of maximum power 100 kW. The centrifugal pump is especially designed to work on the same shaft as the corresponding ORC microturbine. The ORC unit works on R7100 (HFE7100) – a low-boiling fluid characterized by a zero ozone depletion potential coefficient. The pump has the following rated parameters: nominal flow rate of work-ing fluid 4 kg/s, operating rotor speed 10 000 rpm. The pump designed by means of the 0D meanline method is subject to computational fluid dy-namics (CFD) calculations and analysis. The obtained flow field results are discussed and performance characteristics of the pump are presented. The non-cavitating operational region is determined for the pump.

Keywords: CFD; ORC power plant; Microturbine and pump; 0D meanline design

Nomenclature

c – absolute flow velocity, m/s
c – chordwise coordinate, mm
c_u – circumferential component of absolute velocity, m/s

c_m – meridional component of absolute velocity, m/s
D – diameter, mm
h – blade height, mm
h – specific enthalpy, kJ/kg
h_A – total enthalpy, kJ/kg
H – head, m
k_u – speed coefficient
$\dot{m}$ – massflow rate, kg/s
N_{S1} – specific speed
n_{SQ} – hydraulic specific speed
n – rotational speed, rpm
p_A – total pressure, kPa
p – static pressure, kPa
R – radial coordinate, mm
U – blade linear velocity, m/s
$\dot{V}_2$ – outlet volumetric flow rate, m_3/s
w – relative velocity, m/s
x, y – normal plane coordinates, mm
z – axial coordinate, mm

Greek symbols

α – absolute angle, °
β – relative angle, °
δ – diameter ratio
η_{sA1} – efficiency of inlet reducer
η_{s23} – efficiency of diffusor
η_{TS} – efficiency of pump stage
λ – friction factor in diffusor
μ_u – slip factor
τ – dimensionless circumferential speed
τ^* – constructional dimensionless circumferential speed
ϕ – dimensionless meridional speed

Subscripts

ad – adiabatic
u – circumferential
m – meridional
s – isentropic
1 – at impeller inlet
2 – at impeller outlet
3 – at diffuser

Abbreviations

CFD – computational fluid dynamics
HFE – hydrofluoroethers
ORC – organic Rankine cycle
RANS – Reynolds averaged Navier-Stokes

1 Introduction

Recent years have been a period of dynamic development of ORC technol-ogy. Research teams from all over the world work to improve the energy efficiency of ORC systems, including turbines and pumps as main ORC elements [1–5].

Centrifugal pumps are very common devices in the industry. They have many advantages, three of the most important are: simple construction, high efficiency and the fact that they are easy to maintain. Their main elements are: impeller, shaft, bearings, bearing housing, drive coupling and sealing. The principles of construction and methods of design of centrifugal pumps can be found in [6].

A high-speed centrifugal pump was described in [7], where the rotor speed was equal to 13 000 rpm. The authors discussed the effect of blade number on the head coefficient and pump characteristics. Another centrifugal high-speed pump was investigated experimentally and numerically in [8]. The pressure head of this pump converted from the kinetic energy of the liquid was equal to 410 m, whereas the rotor speed was equal to 8500 rpm. The experimental results showed that a back-flow in the impeller has a sig-nificant impact on its performance.

In the majority of ORC systems, the pump and turbine are independent parts of the system [9]. The idea of a small turbine-generator having more than one function was presented in [10]. The author presents a design of the high speed oil free hermetic turbo-generator – feed pump. The efficiency of such an ORC unit was proved to be higher than in the case of separately working pump, turbine and generator. The author tested three prototypes of oil free machines.

Hermetic pumps use working fluid for lubrication. Among the companies that produce hermetic pumps are Hermetic [11] and Allweiler [12]. Their electric motor is connected with the impeller shaft by a magnetic clutch. One of the most sophisticated pumps is produced by the company Tri-O-gen [13]. The working fluid is toluene. The turbine is connected to the pump impeller by a shaft, which makes the ORC unit smaller. The stator of the electric motor is mounted on the shaft and the clutch is not used. Pressure heads up to 3 200 kPa can be reached at the pump end.

Cavitation is a phenomenon that can result in damage of pump im-pellers. Small micro jet implosions damage the surface of the impeller. This phenomenon appears when the local pressure decreases below the satura-tion pressure [15, 16]. The areas of the centrifugal pump where cavitation

usually appears, as well as the discharge and suction recirculation zones, are presented in Fig. 1. The pump requires correct net positive suction head to prevent the cavitation phenomena [17].

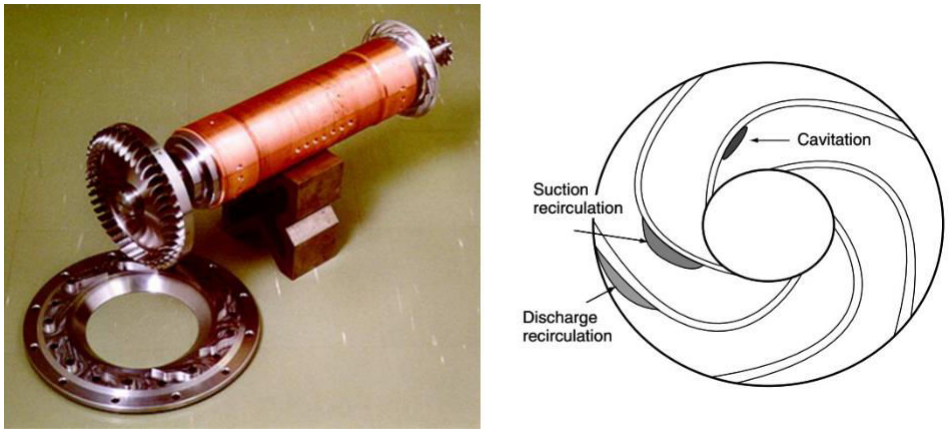

Figure 1: The trio-O-gen turbo-generator with a turbine and pump impeller on the same shaft [14] (left). Regions within the an impeller that are affected by cavitation and recirculation [6] (right).

In this paper the authors pursue the idea of a hermetic turbo-generator and feed pump working on the same shaft with the turbine impeller. The pump is developed for an ORC power unit of 100 kW by means of the 0D meanline method and is investigated with the help of CFD.

2 Feed pump design method

The pump stage was designed using an in-house one dimensional code with the universal design algorithm for compressing machines. The basic differ-ence between the compressor and pump design lies in different coefficients of the working machines. The effect of that difference is pronounced in dif-ferent velocity triangles and geometry of the impellers. The method takes the thermodynamic properties of the working medium operating in the machine both for the liquid and gas phase directly from the Refprop base [18, 19].

The calculation algorithm works in two variants. The dimensionless vari-ant is used when the main dimensions of the machine are not specified; in the majority of cases that method is used when a new machine is designed.

The dimensional variant is used when the main dimensions of the impellers are already set. This second method is usually used when the impeller of the machine is rebuilt.

The pump is a part of the ORC installation, an element that cooperates with the expansion device. The main function of the pump is to assure the required mass flow and pressure conditions for the microturbine, at the same time keeping the volume of liquid so as to prevent cavitation. In our case the pump is working on the same shaft with the turbine impeller. The rotor speed of the pump is equal to the rotor speed of the turbine.

2.1 Design calculations

The algorithm calculations were made for the 100 kW ORC unit working for the assumed nominal operational conditions, including the mass flow rate and rotational speed of the rotor as presented in Table 1. Other in-put parameters and coefficients necessary for design calculations are also collected in this table. Values of calculated output parameters, including dynamic, kinematic and geometrical parameters are in turn gathered in Table 2, whereas velocity triangles for the designed pump impeller are illustrated in Fig. 2. Since the pump rotor is designed to work coupled with the turbine, the pump rotational speed is fixed at 10 000 rpm. On the other hand, the rotational speed is a parameter that can be optimized by the algorithm. If the restriction for the rotational velocity is waived, the algo-

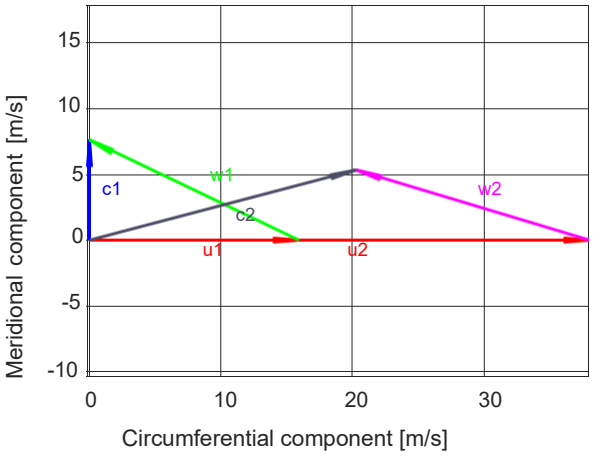

Figure 2: Velocity triangles for the 100 kW ORC pump impeller.

Table 1: Input parameters for the design calculations of the 100 kW ORC pump.

Symbol	Parameter	Value
–	working fluid	HFE7100
–	phase	subcooled liquid
$\dot{m}$	mass flow	4 kg/s
n	rotational speed	10 000 rpm
pA	total pressure at stage inlet	450 kPa
T_A	total temperature at stage inlet	303 K
$\Pi = \frac{p2}{pA}$	stage compression (without diffuser)	2.6
η_{sA1}	efficiency of inlet reducer	1
η_{s23}	efficiency of diffuser	0.6
$\mu_u = \frac{\tau_2}{\tau'_2}$	slip factor	0.93
λ	friction factor in diffuser	0.05
$k_u = \frac{u_2}{\sqrt{2h_{A2s}}}$	speed coefficient	1.23
$\phi 1 = \frac{c_{1m}}{u2}$	dimensionless meridional speed at impeller inlet	0.2
$\phi 2 = \frac{c_{2m}}{u2}$	dimensionless meridional speed at impeller outlet	0.14
$\tau 1 = \frac{c_{1u}}{u2}$	dimensionless circumferential speed at impeller inlet	0
$p3$	diffuser outlet pressure	1264 kPa
$\delta 12 = \frac{u1}{u2} = \frac{D1}{D2}$	ratio of mean diameter	0.42
$D3/D2$	diffuser / impeller ratio	1.2

rithm would prefer a larger value around 13 000 rpm. The assumed lower rotor speed of the pump has the effect of increasing the diameter of the flow path, but also decreasing the blade height, thus leading to more intensive secondary flows and a decrease in flow efficiency. There is a possibility to increase the blade height by changing the dimensionless meridional velocity at the impeller outlet, $\phi 2$, but then the blade angle needs to be changed, having a negative impact on the working area of the pump.

The pump stage efficiency, η_{TS}, was found equal to 70% in the nominal point of work. This efficiency value still does not include losses due to friction of the impeller disc nor losses due to leakage, which can be significant.

s

Table 2: Resultant values of output parameters of the designed 100 kW ORC pump.

Symbol	Parameter	Value
$N_{S1} = \frac{n\sqrt{V_2}}{h_{3/4}}$	specific speed	0.084
$n_{SQ} = \frac{n\sqrt{Q}}{H^{3/4}}$	hydraulic specific speed	31.2
η_{TS}	efficiency of pump stage	0.7
$\tau_2 = \frac{c_{2u}}{u_2}$	dimensionless circumferential speed at impeller inlet	0.57
H	head	54.6 m
p_2	impeller outlet pressure	1170 kPa
c_1	absolute flow velocity at impeller inlet	7.60 m/s
c_2	absolute flow velocity at impeller outlet	20.97 m/s
c_3	absolute flow velocity at diffuser outlet	15.24 m/s
w_1	relative flow velocity at impeller inlet	17.69 m/s
w_2	relative flow velocity at impeller outlet	18.52 m/s
u_1	blade linear velocity at impeller inlet	15.97 m/s
u_2	blade linear velocity at impeller outlet	38.02 m/s
α_1	absolute flow angle at impeller inlet	1.57°
α_2	absolute flow angle at impeller outlet	0.26°
α_3	absolute flow angle at diffusor outlet	0.30°
β_1	relative flow angle at impeller inlet	2.7°
β_2	relative flow angle at impeller outlet	2.9°
h_1	blade height at impeller inlet	3.7 mm
h_2	blade height at impeller outlet	2.2 mm
D_1	impeller inlet diameter	30.5 mm
D_2	impeller outlet diameter	72.6 mm
D_3	diffuser diameter	87.1 mm

2.2 Pump type selection

In order to proceed with the design process let us recall the pump flow diagram presented in Fig. 3 that has been published in [20] showing the areas of application of different pump types. This diagram is drawn in British Imperial Standards, so Table 3 is put forward to gather chosen values found based on Tables 1 and 2 converted to imperial values. To calculate the spe-

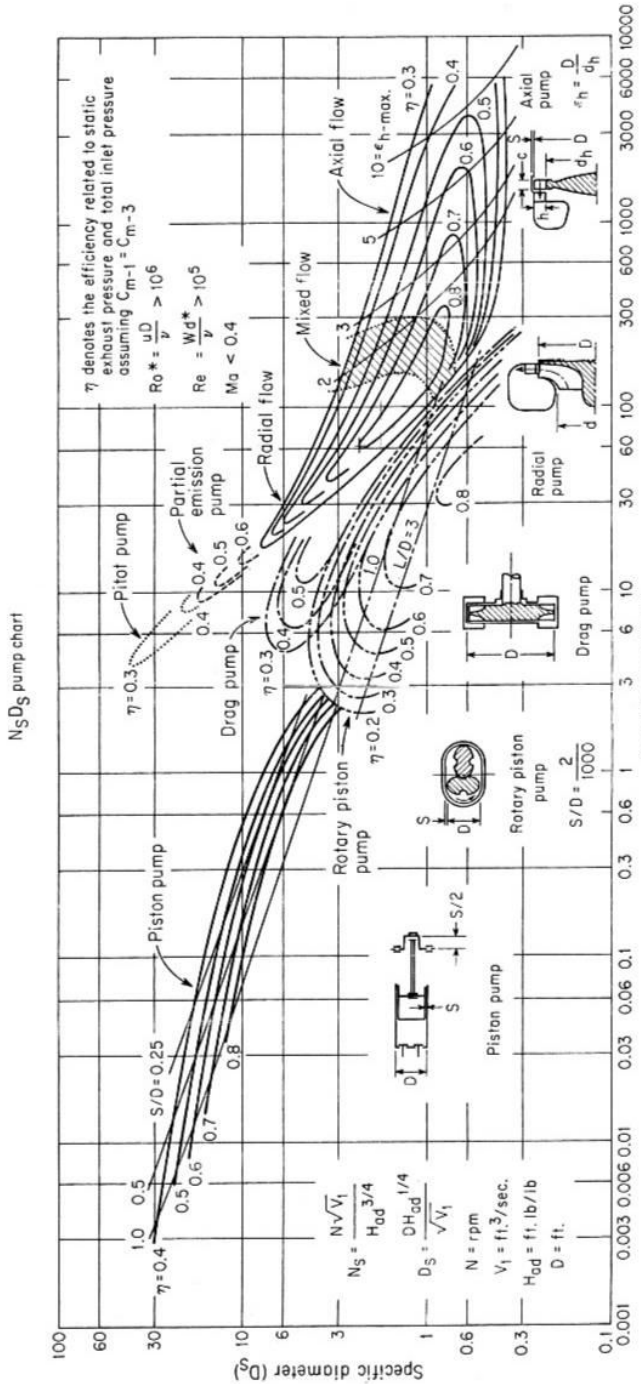

Figure 3: Diagram of pump type selection for different applications [20].

cific speed (N_S) and specific diameter (D_S) requested by the diagram, the following equations can be used:

$$N_S = \frac{N\sqrt{V_1}}{H_{ad}^{3/4}} = \frac{10\,000 \times \sqrt{0.0942}}{179^{3/4}} = 63, \quad (1)$$

$$D_s = \frac{DH_{ad}^{1/4}}{\sqrt{V_1}} = \frac{0.24 \times 179_{ad}^{1/4}}{\sqrt{0.0942}} = 2\,86 \quad (2)$$

Table 3: Resultant values of output parameters of the designed 100 kW ORC pump.

Parameter	Value
Rotational speed	$N = n$ = 10 000 rpm
Diameter	D = 0.0726 m = 2.86 in = 0.24 ft.
Adiabatic head	$H_{ad} = H$ = 54.6 m = 179 ft.
Volumetric flow rate (subcooled liquid HFE7100)	V_1 = 0.00267 m^3/s = 0.0942 ft^3/s

The obtained values of specific speed and diameter assume values that belong to the application area of radial flow pump (centrifugal pump). Within this area the pump exhibits the isentropic efficiency between 70% and 80%, which also agrees with the results of 0D mean-line calculations.

2.3 Pump impeller geometry

The main dimensions and flow angles were used to design flow geometry. The impeller is centrifugal with a diameter of 72.6 mm. The height of the impeller blades is equal to 2.2 mm. The impeller has 6 blades and a 3D geometry. The impeller geometry was generated with the use of a MAT-LAB script [21]. A view on the impeller geometry calculated using the 0D meanline method is presented in Fig. 4.

Meridional endwall contours of the flow channel were determined by means of third-order b-splines and are illustrated in Fig. 5. The channel is quite narrow due to the low blade height of 2.2 mm. The impeller blades were constructed based on two profiles at the impeller hub and tip by means of interpolation between the hub and tip. Hub and tip profiles are built based on the skeletal lines and profile thickness distribution. The skeletal line is defined by a blade angle function along the profiles (profile chords) also in the form of third-order b-splines. The distribution of blade angle for

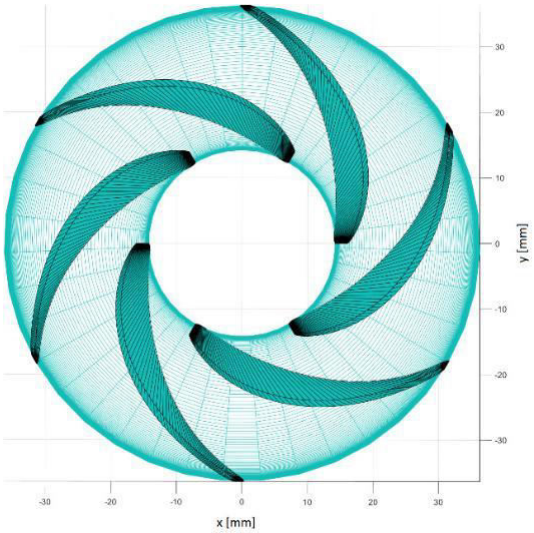

Figure 4: A view on the impeller geometry from its inlet.

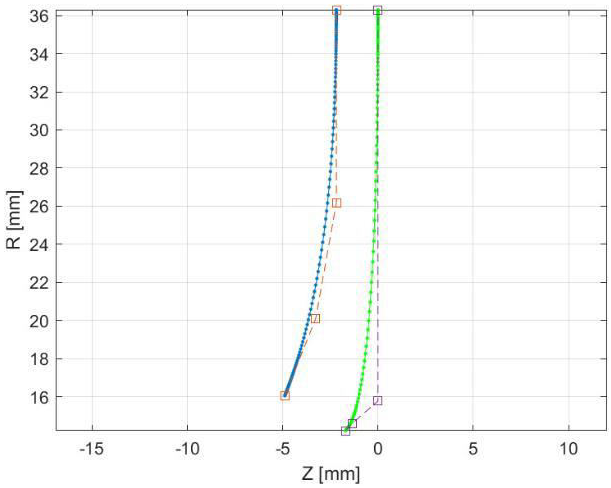

Figure 5: Meridional shape of impeller endwalls within the blades.

the hub and tip profiles is illustrated in Fig. 6. It should be noted that the blade is characterized by a considerable twist about its gravity center line. The distribution of profile thickness at the hub and tip is shown in Fig. 7. This distribution is illustrated in the form of short perpendicular stretches of length proportional to local thickness.

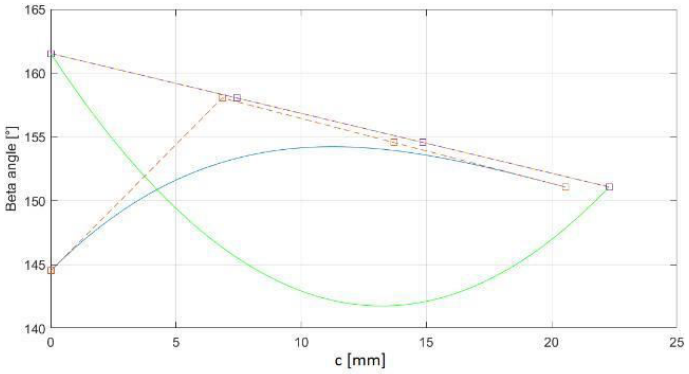

Figure 6: Beta angle distribution along the hub and tip profiles.

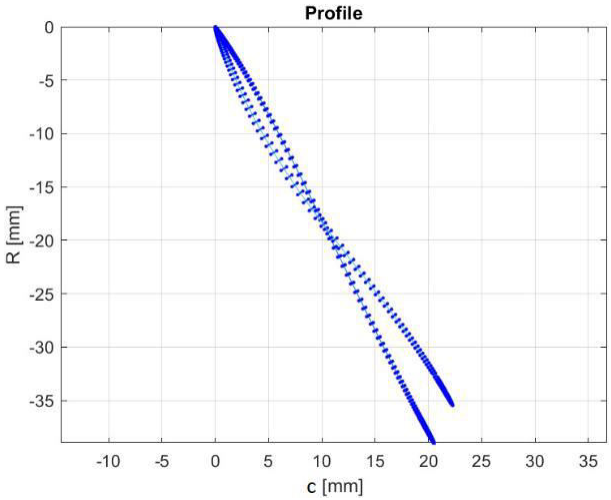

Figure 7: Distribution of profile thickness at the hub and tip.

3 Numerical analysis of pump impeller flow

Numerical investigations aimed at discovering flow phenomena that take place in the pump impeller and identification of areas endangered by cavi-tation.

3.1 Flow solver and mesh

Numerical calculations were carried out with the use of ANSYS software [22]

Steady-state Reynolds averaged Navier-Stokes (RANS) computations

were conducted in CFX application. The *k-ω* SST (shear stress transport) turbulence model was used. 3D flow was analyzed in a single blade-to-blade passage with periodic boundaries. The frozen rotor interface was used between rotating and stationary domains. The assumed numerical scheme was second-order accurate in space and time.

The discretization of the calculation area was prepared in ANSYS Turbo-Grid software[23]. Prepared hexahedral grids were adequately wall-refined. The *y*+ parameter was assumed to be less than 2 and the total number of grid elements was assumed equal to 300 000. A sample 3D view of the computational grid of the pump impeller flow domain is presented in Fig. 8.

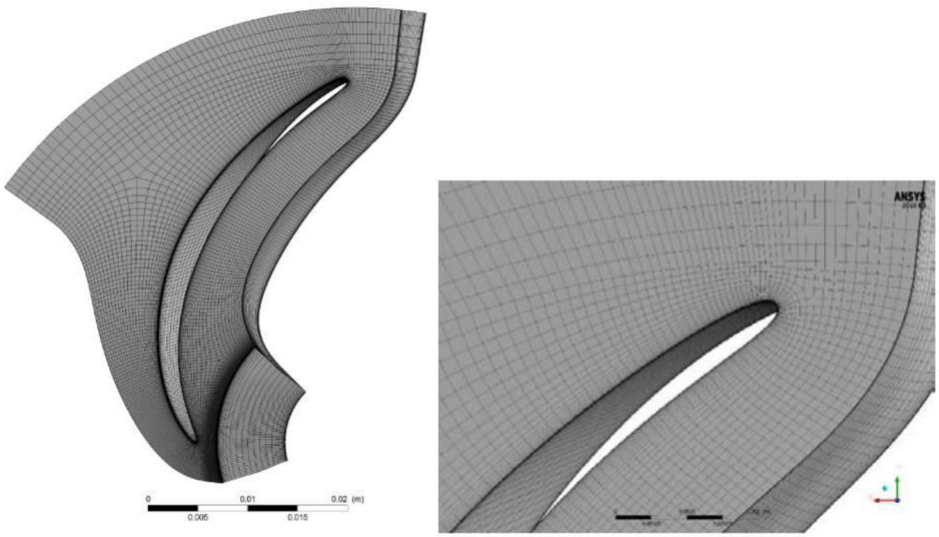

Figure 8: Computational grid of the pump impeller flow domain.

The choice of mesh resolution was preceded by mesh sensitivity studies conducted in a wide range of mesh resolution, between 50 000 and 2 100 000 grid elements. The final decision of the 300 000 element mesh was based on a compromise between the computational costs and accuracy, having satisfied the requirements of the turbulence modelling. As illustrated in Fig. 9, showing variations of pump efficiency and head with the number of grid elements, the discrepancy between the calculation results obtained using 300 000 and 2 100 000 elements does not exceed 0.7% for the pressure head and 0.07% for the efficiency. Therefore, calculations of the pump flow on the computational mesh of 300 000 elements were assumed basically grid independent.

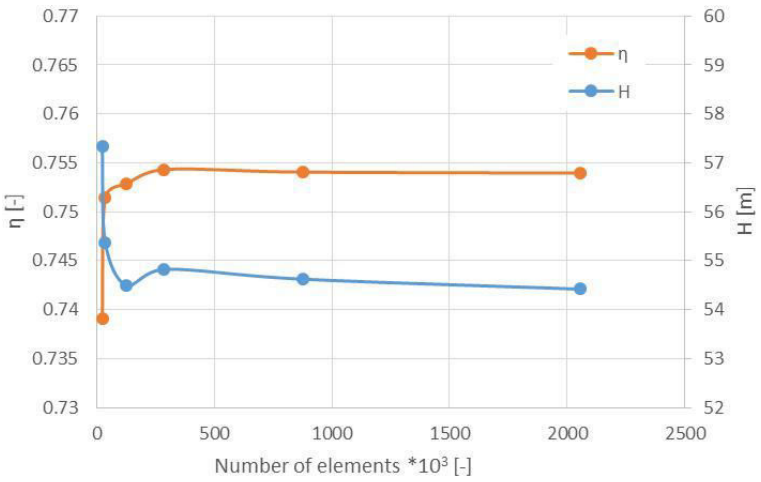

Figure 9: Results of grid independence analysis.

3.2 Numerical results

The presentation of numerical results starts with static pressure contours in the meridional section of the pump impeller blade-to-blade averaged, at the lower endwall and at the blade walls, all illustrated in Fig. 10 for the nominal operating point of the device. Pressure contours are regular. The pictures exhibit zones of low pressure, decreasing below the inlet pressure in the front part of the flow passage near the leading edge at the blade tip's concave surface. However, no pressure drop below 13 kPa is observed, so there is no risk of occurrence of cavitation effects at the nominal operating point.

In comparison, static pressure contours at the endwalls and blade walls for some non-operating points beyond the pump working area (as evaluated in the next chapter) are illustrated in Fig. 11. Pressure drops below 13 kPa can be observed where the process of changing the liquid phase to gas begins, giving rise to cavitation that can lead to damage of the impeller. The cavitation area is typically located at the blade concave surface as a result of flow separation and recirculation near the leading edge. No cavitation area is observed at the convex surface of the pump impeller blades for the mass flow rate of 3 kg/s. The cavitation appears at the convex side of the blade with the flow rate decreasing below 2 kg/s.

The vectors of velocity for nominal flow presented in Fig. 12 exhibit regular unseparated flow on most of the suction and pressure surfaces. Sep-

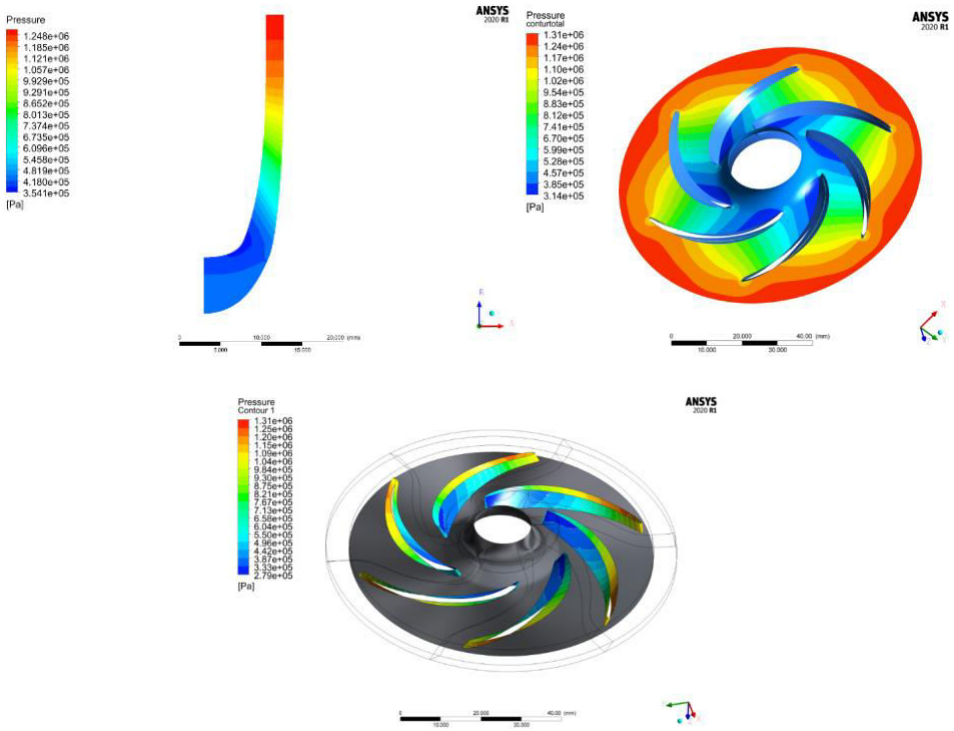

Figure 10: Static pressure in meridional section of the pump impeller blade-to-blade averaged (left), at the lower endwall (right) and at the blade walls (bottom) for the nominal operating point (4 kg/s).

aration areas are visible at the leading edge on the pressure side and at the trailing edge on the suction side of the profile, the former leading to a considerable pressure drop and risk of cavitation. Total pressure contours in the pump impeller illustrated in Fig. 13 for nominal flow show decreased values at the trailing edge of the blade and downstream. The overall total pressure loss is cumulated in the trailing edge wake area. Nonetheless the flow seems regular.

The isentropic efficiency of the pump impeller obtained from computational fluid dynamics (CFD) calculations for nominal operating conditions is equal to about 77%, which exceeds by 7% point the value obtained from the 0D meanline model. The 0D model seems to overestimate the level of loss from the superposition of loss correlation models. Let us also recall that both the 0D model and CFD model do not take into account leakage flows nor friction against shaft and impeller disc. Therefore, the expected

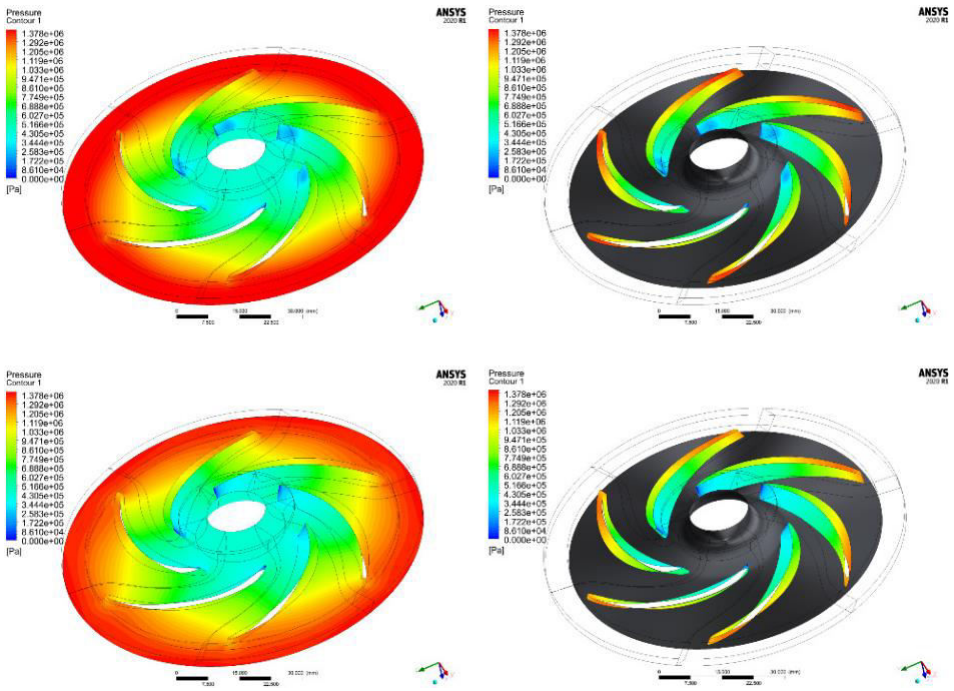

Figure 11: Static pressure at the lower endwall (left) and at the blade walls (right) for some non-operating points: head – 100 m, flow rate – 2 kg/s (top), head – 93 m, flow rate – 3 kg/s (bottom).

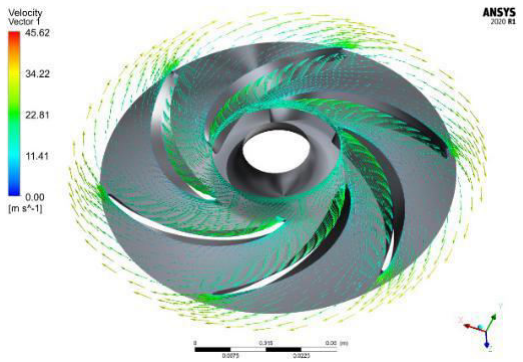

Figure 12: Velocity vectors in the pump impeller coloured by velocity magnitude for the nominal operating point (4 kg/s).

efficiency of the manufactured machine will still be lower. In general, the obtained results of CFD calculations show correct inflow of fluid on impeller

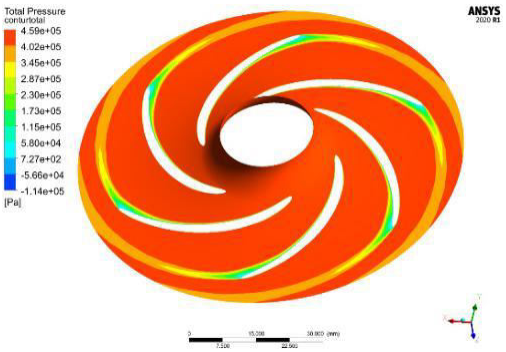

Figure 13: Total pressure contours in the pump impeller for the nominal operating point (4 kg/s).

blades and correct downstream flow. Possibly, some moderate changes in blade angle distribution can be made in the front part of the blade tip profile to reduce the extent of cavitational flow for off-design areas and to widen the pump working area.

4 Performance characteristics of the pump

The rotational speed of the pump in nominal operating condition remains fixed and equal to the turbine rotor speed. However, full performance characteristics are necessary for control of the ORC system in transient states, including start-up, shut-down and instability of external heat source. With this respect, the admitted working area of the pump impeller must be evaluated. Long work beyond this area can lead to early damage of the pump impeller and can also be hazardous for the whole ORC installation.

In this section, characteristics of the pump impeller for the 100 kW ORC unit are presented in Fig. 14 as a function of mass flow rate and angular velocity as a parameter. The characteristics include the impeller pump power, efficiency, and hydraulic head versus mass flow rate. CFD calculations were conducted in the range of mass flow rate up to 5.5 kg/s and for five rotational velocities of 4 000, 6 000, 8 000, 10 000, 12 000 rpm. Further increasing the rotational speed makes the lines of characteristics shorter, the impeller pump has a smaller area of regulation and the situation remains beyond the scope of application.

Power and efficiency characteristics are relatively flat for higher rotational speeds (above 8 000 rpm). With the increasing mass flow rate the

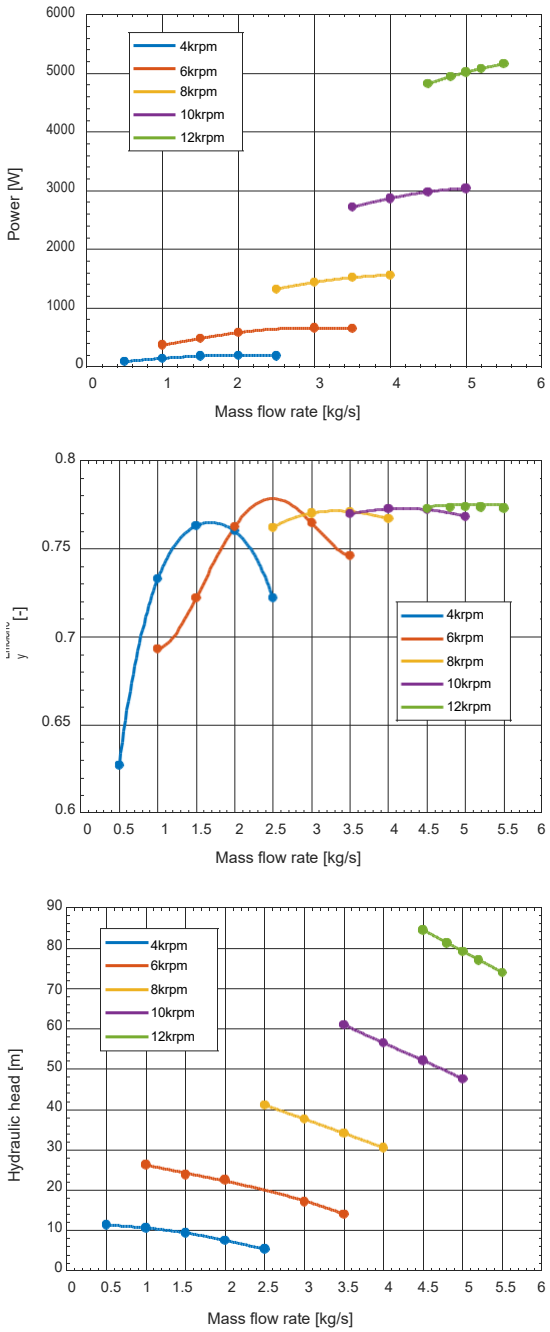

Figure 14: Power (top), efficiency (centre) and hydraulic head (bottom) characteristics of the pump impeller for the investigated 100 kW ORC unit.

hydraulic head is decreased. The hydraulic head is increased by increasing the rotational velocity. Similar trends can be observed in [24, 25].

The map of efficiency and working area of the pump for the 100 kW ORC unit are illustrated in Fig. 15. The area of highest efficiency is relatively wide and is located along the diagonal of the hydraulic head/mass flow rate variation. Lower efficiency areas are those of low mass flow rate or low hydraulic head. The working area of the investigated pump is located between the continuous black solid lines. This is the non-cavitating area of operation.

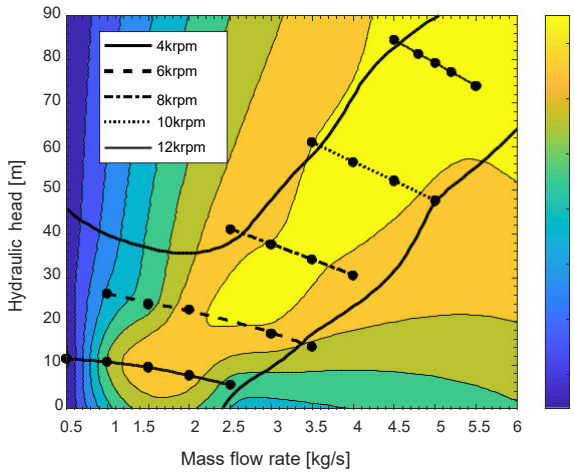

Figure 15: The map of efficiency and working area of the pump for the 100 kW ORC unit.

5 Summary

A prototype centrifugal pump for an ORC power plant of maximum power 100 kW working on R7100 (HFE7100) has been designed by means of the 0D meanline method. This centrifugal pump (of the following rated parameters: nominal flow rate of working fluid 4 kg/s, pressure ratio – 2.6) is dedicated to work on the same shaft as the corresponding ORC microturbine, operating with the nominal rotor speed of 10 000 rpm. This assumption has imposed an increased diameter of the flow path and a lower height of the blade as compared to the theoretically optimum pump design with the optimum rotational velocity around 13 000 rpm, preferred by the 0D meanline method. The flow efficiency of the pump for nominal operating conditions

was evaluated at 70%, not including friction of the impeller disc nor losses due to leakage.

The designed pump has been subject to CFD calculations and analysis. The flow efficiency from RANS simulations was updated to 77% (nominal flow). The enclosed pressure contours and velocity vectors illustrate the process of compression. The flow is free from cavitation for nominal operating conditions. The pressure drops below 13 kPa for mass flow rate of 3 kg/s at the blade concave surface as a result of flow separation and recirculation near the leading edge, giving rise to cavitation there. No cavitation area is observed at the convex surface of the pump impeller blades at this flow rate. However, with the further decreasing flow rate, the convex side of the blade also becomes prone to cavitation.

Performance characteristics of the pump, including hydraulic head, power, and efficiency versus mass flow rate, as well as the map of efficiency and working area of the pump have been evaluated. The working area is a non-cavitating operational region and remains relatively wide. A large part of this area belongs to the region of highest efficiency.

Acknowledgements The investigations have been supported by the BIO-STRATEG project that has received funding from the Polish National Cen-tre for Research and Development (NCBR) under Grant Agreement Num-ber BIOSTRATEG3/344128/12/NCBR/2017.

Received 6 October 2020

References

[1] Quoilin S., Van Den Broek M., Declaye S., Dewallef P., Lemort V.: *Techno-economic survey of organic rankine cycle (ORC) systems*. Renew. Sustain. Energy Rev. **22**(2013), 168–186. doi: 10.1016/j.rser.2013.01.028.

[2] Mocarski S., Borsukiewicz-Gozdur A.: *Selected aspects of operation of supercritical (transcritical) organic Rankine cycle*. Arch. Thermodyn. **36**(2015), 2, 85–103. doi: 10.1515/aoter-2015-0017.

[3] Wajs J., Mikielewicz D., Bajor M., Kneba Z.: *Experimental investigation of domes-tic micro-CHP based on the gas boiler fitted with ORC module*. Arch. Thermodyn. **37**(2016), 3, 79–93. doi: 10.1515/aoter-2016-0021.

[4] Borsukiewicz-Gozdur A.: *Pumping work in the organic Rankine cycle*. Appl. Therm. Eng. **51**(2013), 1–2, 781–786. doi: 10.1016/j.applthermaleng.2012.10.033.

[5] Macchi E., Astolfi M. (Eds.): Organic Rankine Cycle (ORC) Power Systems: Technologies and Applications. Elsevier 2017.

[6] Girdhar P., Moniz O., Mackay S.: *Practical Centrifugal Pumps*. Elsevier, 2005. doi: 10.1016/B978-0-7506-6273-4.X5000-4.

[7] Jafarzadeh B., Hajari A., Alishahi M.M., Akbari M.H.: *The flow simulation of a low-specific-speed high-speed centrifugal pump*. Appl. Math. Model. **35**(2011), 1, 242–249. doi: 10.1016/j.apm.2010.05.021.

[8] Cui B., Zhu Z., Zhang J., Chen Y.: *The flow simulation and experimental study of low-specific-speed high-speed complex centrifugal impellers*. Chinese J. Chem. Eng. **14**(2006), 435–441. doi: 10.1016/S1004-9541(06)60096-7.

[9] Eyerer S., Dawo F., Wieland C., Spliethoff H.: *Advanced ORC architecture for geothermal combined heat and power generation*. Energy **205**(2020), 117967. doi: 10.1016/j.energy.2020.117967.

[10] Larjola J.: *Electricity from industrial waste heat using high-speed organic Rankine cycle (ORC)*. Int. J. Prod. Econ. **41**(1995), 1-3, 227–235. doi: 10.1016/0925-5273(94)00098-0.

[11] Lederle Hermetic, (2020). www.hermetic-pumps.pl/marki-i-produkty/hermetic/ (accessed 30 June 2020).

[12] Allweiler Company, (2020). www.allweiler.de/en (accessed 30 June 2020).

[13] Triogen, (2020). www.triogen.nl/technology/triogen-high-speed-turbo-generator (accessed 30 June 2020).

[14] Jos van Buijtenen: *Design, Development & Operation of the Tri-O-Gen ORC Power Unit*. In: Proc. 1st Int. Semin. ORC Power Syst., Delft, 2011.

[15] Bai L., Yan J., Zeng Z., Ma Y.: *Cavitation in thin liquid layer: A review*. Ultrason. Sonochem. **66**(2020), 105092. doi: 10.1016/j.ultsonch.2020.105092.

[16] Brennen C.E.: *Cavitation and Bubble Dynamics*. Cambridge University Press, Cambridge 2013. doi: 10.1017/CBO9781107338760.

[17] Bachus L., Custodio A.: *Know and understand centrifugal pumps by Larry Bachus and Angel Custodio*. Elsevier, 2003.

[18] Lemmon E.W., Huber M.L., McLinden M.O.: NIST Standard Reference Database 23: Reference Fluid Thermodynamic and Transport Properties (REFPROP), Version 9.0, Phys. Chem. Prop. (2010).

[19] iNVENTEC performance chemicals, NOVEC 7100, Data Sheet. (n.d.). www.inventecusa.com/assets/novec-7100.pdf (accessed 17 Nov. 2020).

[20] Keneth E., Nichols P.E.: *How to Select Turbomachinery For Your Application How to Select Turbomachinery For Your Application*. Barber–Nichols Inc., 2010.

[21] The Mathworks Inc., MATLAB R2018a, www.Mathworks.Com/Products/Matlab (2018). doi: 2016-11-26.

[22] ANSYS R Realase 2020R1, Academic Research CFX, (n.d.). www.ansys.com.

[23] ANSYS R Realase 2020R1, Academic Research TurboGrid, (n.d.). www.ansys.com.

[24] Anagnostopoulos J.: *CFD analysis and design effects in a radial pump impeller*. Wseas Trans. Fluid Mech. **1**(2006), 7, 763–770.

[25] Dick E., Vierendeels J., Serbruyns S., Vande Voorde J.: *Performance Prediction of Centrifugal Pumps With Cfd-Tools*. Task Q. **5**(2001), 4, 579–594.